Seismic Response of Floating Roof Storage Tanks Contact Pressure Analysis

By
Philip J. Cacciatore[1]
L. Magnus Gustafsson[1]
Alexander Kozak[2]

Abstract

Seismic response of liquid storage tank floating roofs involve phenomena that require dynamic nonlinear geometric and material behavior as well as surface to surface contact. Good engineering practice requires a practical analytical approach that captures the essential ingredients of structural behavior under earthquake excitation by making reasonable, conservative, and manageable approximations to the actual conditions. This paper discusses an approach used in Abaqus to calculate the stresses and deformations of a liquid storage tank floating roof under seismic loading. It represents a novel application of contact theory to achieve a solution to this problem. The method is validated by a fully coupled fluid-structure interaction (FSI) finite element analysis using actual earthquake ground accelerations. The method is supported by both the American Petroleum Institute (API) and the Petroleum Association of Japan (PAJ).

Introduction,

The large capacity liquid storage tank is an important facility for the storage of pre-production raw materials and partially or completely processed products for the petrochemical industry. These structures are primarily cylindrical in shape, with a very flexible bottom plate and either a fixed, floating, or combination of fixed and floating roofs. The underlying foundation for the tank can be asphalt, concrete, pre-designed or natural soil support, or crushed stone. These tanks are used to store many different types of hazardous and volatile liquids such as crude oil, naphtha, and gasoline.

The storage tank is a relatively simple welded or riveted structure but it responds to most loadings in a highly nonlinear manner. Beyond the basic hydrostatic loading of the contents, it can be subjected to large deflections and buckling from foundation settlement, wind, rain, snow, and seismic loading. These loads can induce localized plastic deformations in the tank bottom plate, shell walls, and roof.

The focus of this paper is the seismic liquid sloshing response of floating roof storage tanks (Figure 1). Seismic loading will induce both impulsive (fluid mass) and convective (liquid sloshing) loads on the tank walls. Simplified seismic design attempts to minimize the effects of these loadings which generate shearing and overturning forces on the tank. Primary mitigation methods of seismic effects rely on anchoring systems based on a seismic design spectrum. Earthquake loading is random and can be so powerful in magnitude that anchoring systems can and often fail. Inadequate design could result in loss of containment integrity or the more unusual "walking away" off the foundation and a phenomena known as "elephant foot buckling" (Cacciatore, 2004). Floating roof tanks are particularly vulnerable to

[1] ExxonMobil Research & Engineering Co., 3225 Gallows Road, Fairfax, Virginia, 22037-0001, USA
[2] SC Solutions Inc. 1261 Oakmead Parkway, Sunnyvale, CA 94085, USA

seismic events since the displacement of the roof is driven by the induced sloshing waves generated on the liquid surface (Kikuchi, 2005). If key floating roof components fail and roof buoyancy is lost, the roof will sink, exposing the environment to the hazardous material and creating the potential for a fire and/or explosions. If the seismic effects can not be mitigated, liquid levels must be lowered to reduce the seismic impulsive loadings and the sloshing wave effects on the roof. This can result in a significant reduction in capacity with a corresponding economic impact.

Contact Pressure Approach (CPA)

The analysis of a single floating roof tank under seismic loading subject to all the nonlinear behavior described above is a formidable task. Engineering analysis requires a practical analytical approach that captures the effects of the seismic loading by making reasonable, conservative and manageable approximations to the actual conditions. The goal is simply to obtain results that can guide design and design modifications and maintain an adequate safety level. ABAQUS provides the necessary tools to implement an approach based on standard finite element modeling and surface contact algorithms.

The Contact Pressure Approach (Cacciatore, 2009) described in this paper uses the Velocity Potential theory as a starting point for the analysis (ASCE Technical Council, 1984). Velocity Potential is a linear theory that is limited in scope. The Japanese Fire Disaster Management Agency, due to their strong interest in the damage from seismic response, has completed numerous studies and experiments on floating roof tanks. These have resulted in the addition of a nonlinear component to the linear Velocity Potential Theory (Japanese Fire Disaster Management Agency, March 2006) (In Japanese). The modified equations formed the basis for additions to the Japanese Fire Service Law (FSL) (Yamauchi, 2006), and they are used in a simplified spreadsheet based analysis.

Based on the frequency content of most earthquakes and typical tank-liquid systems, a modal synthesis of the response of the first and second modes of sloshing will capture the main characteristics of the overall response. The modified Velocity Potential equations for 1st ($\eta_1(r,\theta)$) and 2nd mode ($\eta_2(r,\theta)$) sloshing are shown in equation form below and graphically in Figures 1 and 2. Note that the rigid body motion of the mode has been removed (-r/R) and the displacement shapes are just deviations from the rigid body plane.

$$\eta_1(r,\theta) = \beta * (\eta_{\max}^{(1)} \cos\theta + 0.8 * R * (\frac{\eta_{\max}^{(1)}}{R})^2 \cos 2\theta)(\frac{J_1(\lambda_1 \frac{r}{R})}{J_1(\lambda_1)} - \frac{r}{R}) \quad \ldots (1)$$

$$\eta_2(r,\theta) = \alpha * \eta_{\max}^{(2)} \left(\frac{J_1(\lambda_2 \frac{r}{R})}{J_1(\lambda_2)} - \frac{r}{R} \right) * \cos\theta \quad \ldots (2)$$

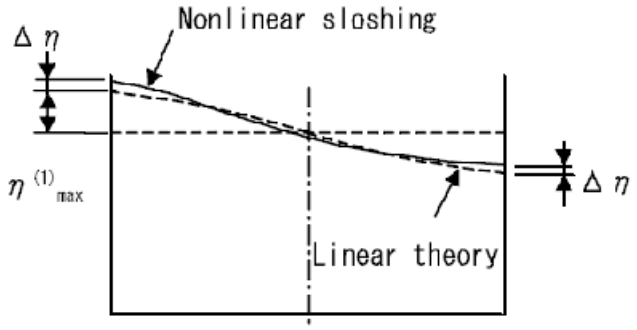

Figure 1. Mode 1 linear & nonlinear sloshing components.

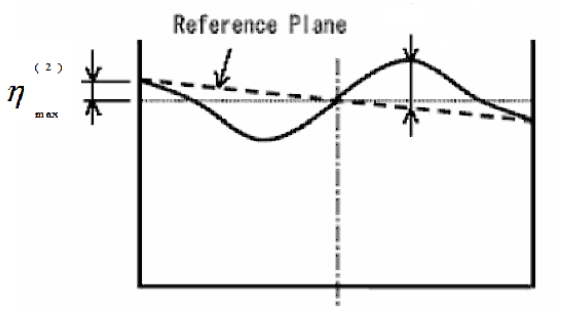

Figure 2. Mode 2 linear sloshing component.

The basic equations have been further modified by ExxonMobil with the addition of two factors, α and β, which represent the attenuation fraction for each mode. The attenuation factors modify the response to account for the attenuation of the free surface sloshing wave by the presence of the floating roof on the liquid surface. The second term (shown in red) in Equation 1 is $\Delta\eta$ and the coordinate system is polar (r,θ). The function J_1 is the standard 1st order Bessel function, and the λ_j are the roots of the derivative of the 1st order Bessel functions. The key parameters in the Mode 1 and 2 sloshing wave equations are $\eta^{(1)}_{max}$ and $\eta^{(2)}_{max}$. These values are the maximum sloshing height at the tank wall for each mode. These parameters, which are based on the Velocity Potential Theory, are provided below:

$$\eta^{(1)}_{\max} = \frac{D}{2g} * \frac{2}{\lambda_1^2 - 1} * \left(\frac{2\pi}{\mathrm{T}_1} \right) * S_v^{(1)} \qquad \text{... (3)}$$

$$\eta^{(2)}_{\max} = \frac{D}{2g} * \frac{2}{\lambda_2^2 - 1} * \left(\frac{2\pi}{\mathrm{T}_2} \right) * S_v^{(2)}$$

$$\omega_j^2 = \frac{\lambda_j g}{R}\tanh(\lambda_j \frac{H}{R})$$

$$T_j = \frac{2\pi}{\omega_j}$$

λ_j = *jth* root of the derivative of the 1st order Bessel Function

R = radius of the tank

H = height of liquid in the tank

where T_1, T_2, $S^{(1)}_v$, and $S^{(2)}_v$ are respectively the periods of vibration for the 1st and 2nd mode tank-liquid system and the pseudo velocity spectrum values corresponding to a frequency sweep (Duhamel Integral evaluation) of the ground acceleration data. D is the tank diameter and g is the acceleration of gravity. Note the dependence of the period on the liquid height and the corresponding dependence of sloshing wave height on period.

Figure 3 contains a comparison between Fluid Structure Interaction (FSI) analysis and Velocity Potential Theory for Mode 1. The FSI analysis is performed with ADINA and employs fluid potential based elements. The FSI results are inherently linear in approximation (frequency and mode shape calculation are inherently a linear perturbation process). The FSI results show good agreement with Velocity Potential Theory linear results.

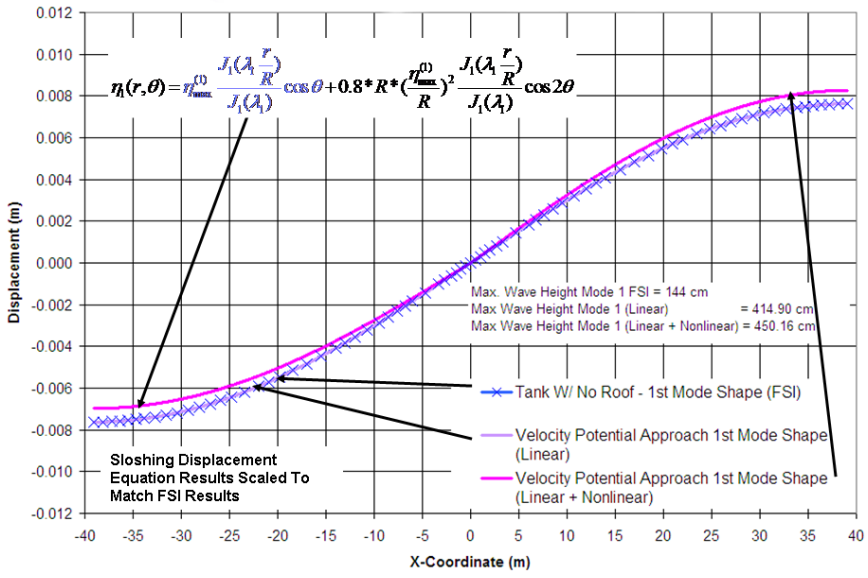

Figure 3. First mode comparison velocity potential & fluid-structure interaction models.

Figure 4 shows a similar comparison for Mode 2. Both of these calculations are validation of the FSI model.

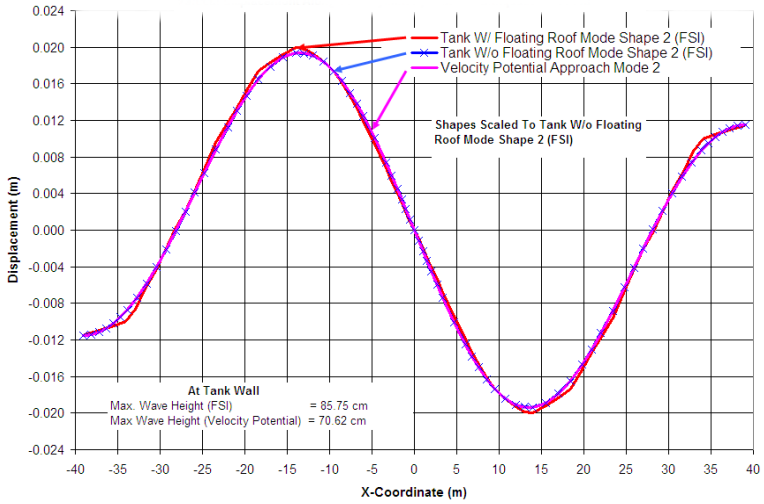

Figure 4. Mode 2 comparison of velocity potential & fluid-structure interaction models

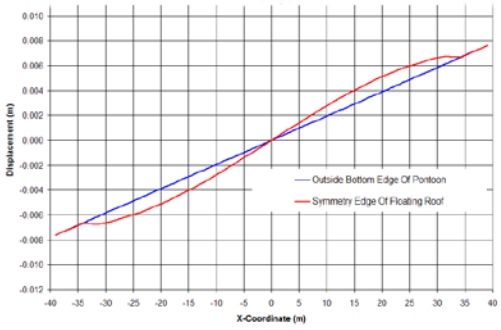

Figure 5. Mode 1 FSI w/ floating roof.

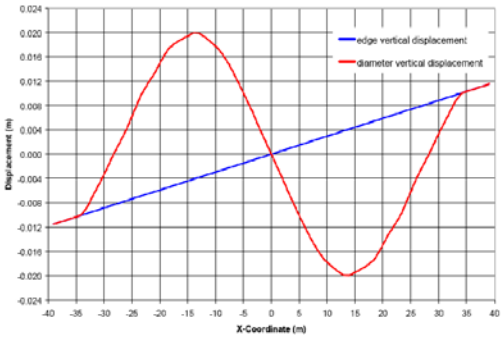

Figure 6. Mode 2 FSI w/ floating roof.

Figures 5 and 6 contain Modes 1 and 2 with the floating roof included in the FSI model. The general form of Modes 1 and 2 are apparent however, the presence of the pontoon introduces a discontinuity in the smooth Velocity Potential mode shapes. The floating roof deck (center plate) is flexible enough to follow the sloshing wave. The pontoon structure is however fairly rigid and appears to simply undergo rigid body motion. In the θ direction, the pontoon has a finite bending rigidity and is immersed in the sloshing liquid. There is a variation in the pressure on the pontoon which is proportional to the difference in the immersion depth and the $\Delta\eta$ nonlinear component of Mode 1. The pontoon displacement from the rigid plane can be developed by examining the deformation of ring beam subject to a uniform load (Japanese Fire Disaster Management Agency, March 2006).

$$PontoonDisplacement = (1-\varphi)\Delta\eta * J_1(\lambda_1 \frac{r}{R}) / J_1(\lambda_1) \text{ .... (4)}$$

$$where \quad \varphi = \frac{k}{\left[\frac{8EI_\theta}{R^4} + k\right]}$$

k = (Pontoon Width)*density

The larger the bending rigidity ($\frac{8EI_\theta}{R^4}$), the smaller φ will be and the displacement approaches Δη (nonlinear component of Mode 1 sloshing wave). Eliminating Δη from the sloshing wave leaves the pontoon with rigid body motion only.

The key ingredients in the sloshing wave equations are sloshing wave heights at the tank wall, i.e. $\eta_{\max}^{(1)}, \eta_{\max}^{(2)}$. These quantities must be closely monitored in the analysis since they can exceed the distance between the static liquid surface and the top of the tank wall (freeboard distance). This is an indication of an overflow/spillage condition which has implications for the sloshing wave effects on the floating roof. It is conservative to ignore the overflow condition, but it can easily be accounted for in the analysis by assuming the actual wave height at the wall can only reach a maximum value equal to the freeboard. Using this assumption, the component modes can be adjusted to stay within that limitation.

The contact pressure concept is used in two separate phases of the analysis. The first phase consists of determining the attenuation factors for the individual sloshing modes. The second phase is the process of modal synthesis (usually square root sum of the squares) of the two main sloshing modes and applying the modal deformations to the floating roof. The following summarizes the Contact Pressure Approach for calculating attenuation factors:

1. The attenuation factor for each mode depends upon:
    a. Pontoon Geometry
    b. Deck Stiffness
    c. Velocity Spectrum Values - $S_v^{(i)}$ which depend on the natural period of vibration for the tank-liquid modes (T_i) which, in turn, depends on among other things the tank diameter and liquid height.
2. Using the Velocity Potential Theory for sloshing wave displacements of the floating roof precludes buckling of the roof components in contact with the liquid. Imposing displacements on the roof is not realistic. A displacement controlled application of the sloshing wave needs to be replaced by a "sloshing pressure" which will give the roof the opportunity to respond to the sloshing wave in a physically realistic manner.
3. CPA Process - Determination of α and β Modes 1 & 2 Attenuation Factors

a. A membrane is placed under the floating roof (Figure 7). Structural details of a typical roof are shown in Figure 8.
b. The floating roof is allowed to settle onto to the membrane.
c. As the roof passes through the membrane, the membrane develops a contact pressure proportional to the distance the roof sinks past the membrane. Contact Pressure = ρg x distance.
d. The contact pressure equalizes to the weight of the roof. This is the buoyant state of the floating roof. Figures 9 & 10 show the contact "buoyancy" pressure and displacement from dead weight loading.
e. The membrane is now displaced incrementally into one of the sloshing "mode shapes". At each increment of displacement, the contact pressure between the membrane and roof is calculated. The membrane can be displaced into either the Mode 1 or Mode 2 sloshing wave. Figure 11 shows the contact pressure at a fraction of the full Mode 1 sloshing wave.
f. The Mode 1 shape has a high and low points at θ=0° and 180° on the symmetry plane, The "red" areas of Figure 11 indicate areas of high pressure and the white areas represent no pressure or loss of contact.
g. The blue areas indicate areas of "low" pressure and these will occur in two possible locations:

    - Where the deck has buckled and possibly separated from the liquid surface.
    - Where the perimeter of the pontoon may be "lifting out" of the liquid.

h. The CPA method can predict the "potential" for pontoon-liquid separation. This opens the possibility of liquid escaping onto the deck or spilling over the tank top and down the outside tank walls. However, separation can occur without spillage. Mode 1 produces the highest wave height at the tank wall. Figure 12 show the Mode 1 formation and shape minus rigid body motion.
i. The white area along the edge of the pontoon in Figure 11 indicates a zero contact pressure (loss of contact) condition for this point in time. If we go backwards in time (reducing the fraction of the wave) to that point where the loss of contact develops, we can use the wave fraction to set the attenuation factor for Mode 1. Keep in mind the true behavior is dynamic and as soon as the loss of contact occurs along the periphery in Mode 1, fluid will rush in to equalize the pressure under the pontoon.
j. A zero pressure on the bottom of the floating roof is not physically realistic. The higher pressure areas of the wave will collapse and push liquid into the lower pressure regions. This prevents the wave from reaching its maximum wave height resulting in "attenuation" of the modal response.
k. For Mode 2, the membrane is displaced incrementally into the Mode 2 displacement pattern and the contact pressure monitored on the bottom of the roof.
l. Figure 13 contains the Mode 2 sloshing wave position following the initial buoyancy establishment of weight equilibrium.
m. Certain zones under the roof continue to develop pressure according to the ρg x distance relation (pressure-over-closure relationship). This is the wave crest.
n. Other zones of the roof will experience a decrease in pressure since the wave is moving away from the roof. This is the wave trough.

o. The roof will follow the wave crest. However, it can only follow the wave trough as far as physically possible (via gravity). At that point the roof will become a catenary over the trough and the contact pressure will go to zero.
p. The fraction of the imposed Mode 2 sloshing wave on the membrane at the point of initial zero contact pressure will set the attenuation factor.
q. Once again, fluid pressures in the crest area will drive fluid into the trough in attempt to equalize underneath the roof.
r. It is important to keep in mind that these are dynamic events that are treated statically. If the event is very slow, the collapse will begin earlier than if the wave formation was a high speed event.
s. Note that the bottom of the floating roof (including the bottom of the pontoon) is allowed to buckle. This would not be possible if the sloshing wave's displacements were imposed directly on the bottom of the roof.
t. If the roof is able to achieve the full sloshing wave (Mode 1 or 2) without developing zero contact pressure there is no attenuation. If the nonlinear incrementation of the sloshing wave fails before there is loss of contact, then the roof has buckled and failed.

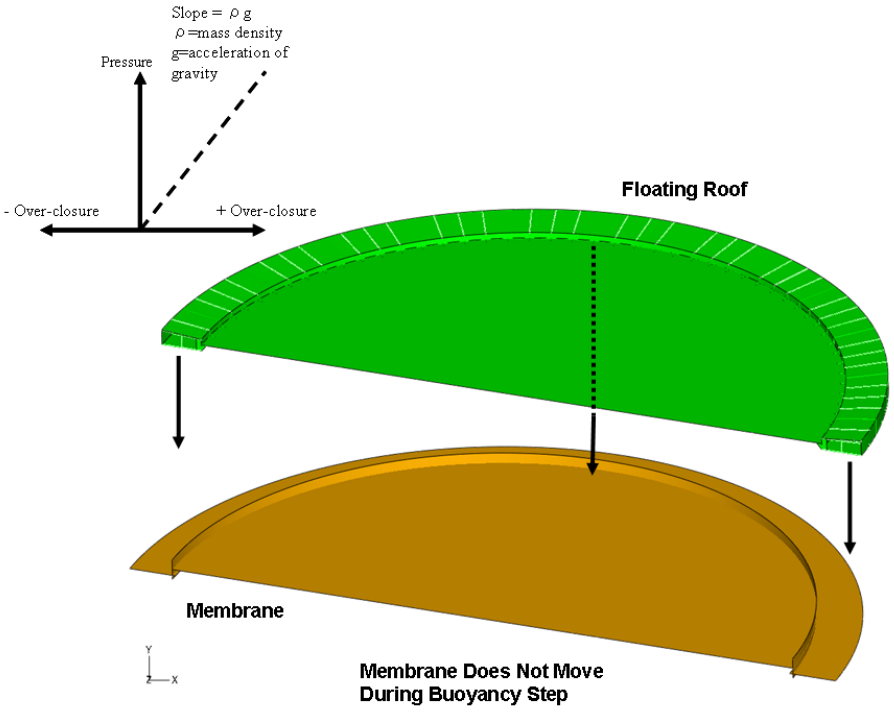

Figure 7. Dead weight loading of floating roof on to membrane.

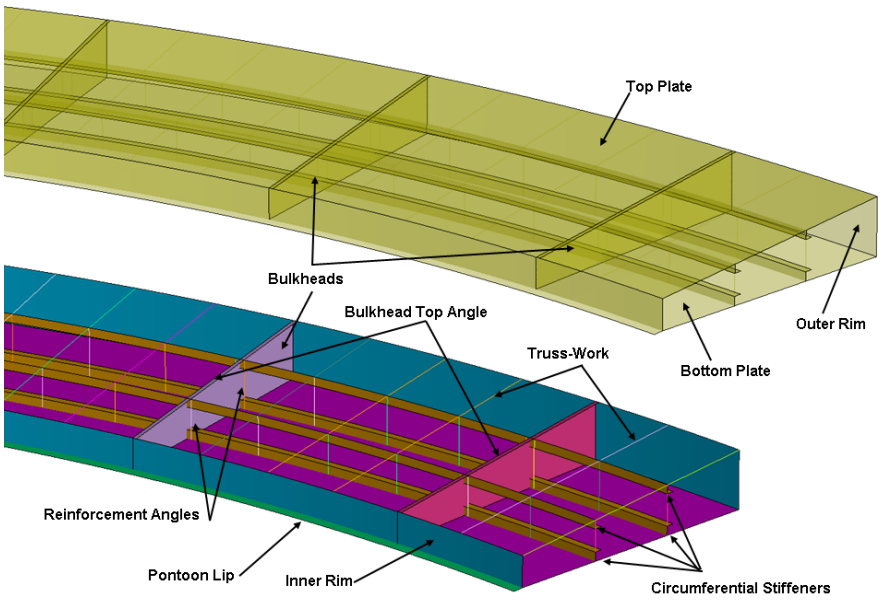

Figure 8. Details of typical pontoon structure.

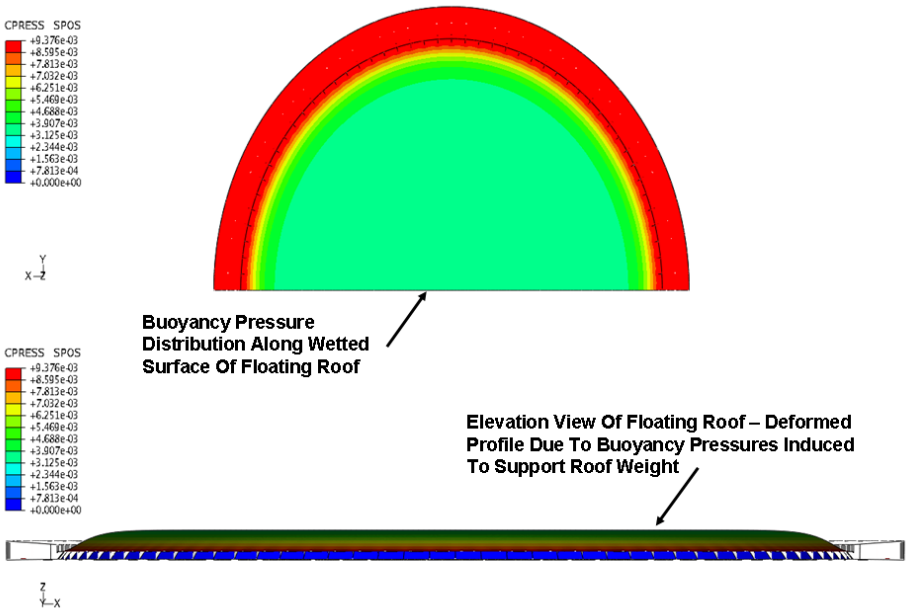

Figure 9. Dead weight pressure distributions on floating roof.

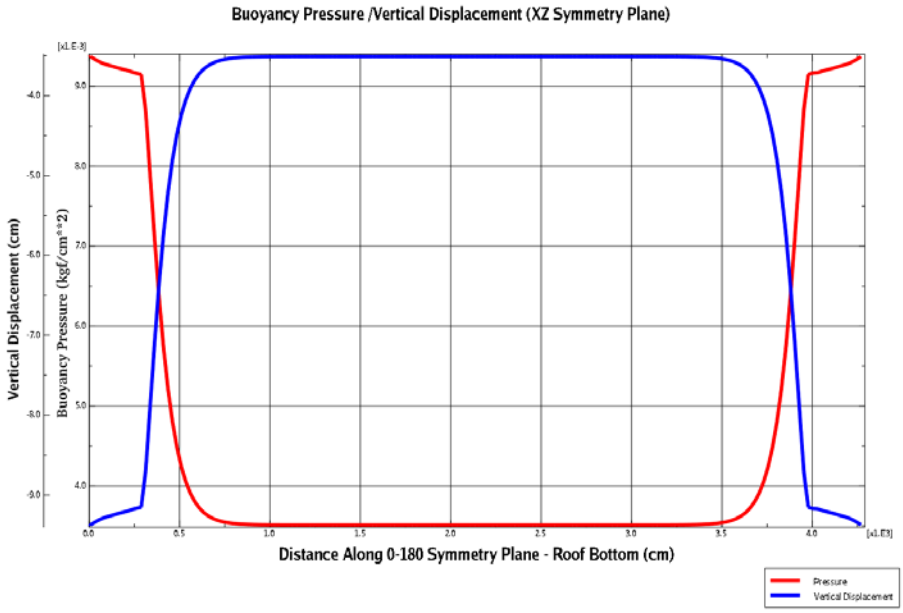

Figure 10. Buoyancy pressure and displacement along symmetry plane of roof.

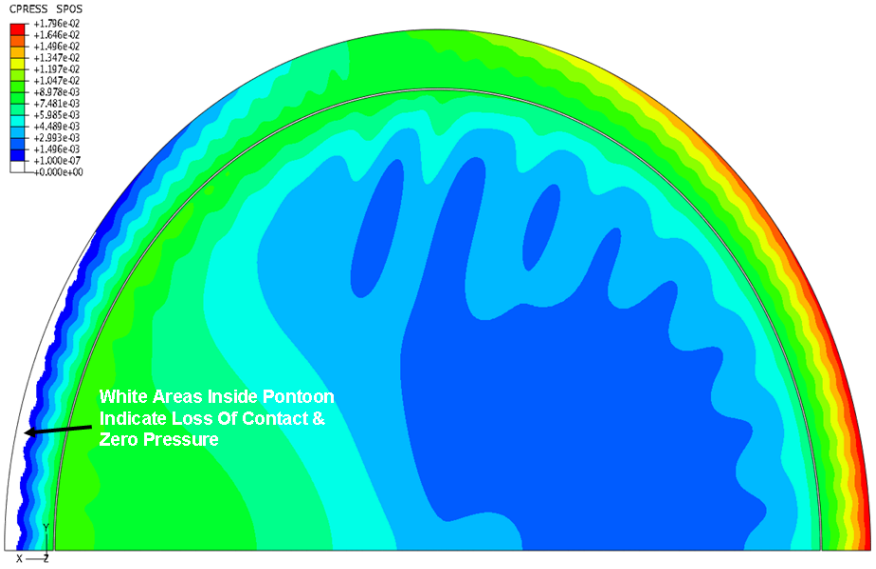

Figure 11. Contact pressure on floating roof at 31.1% of fully developed mode 1 sloshing.

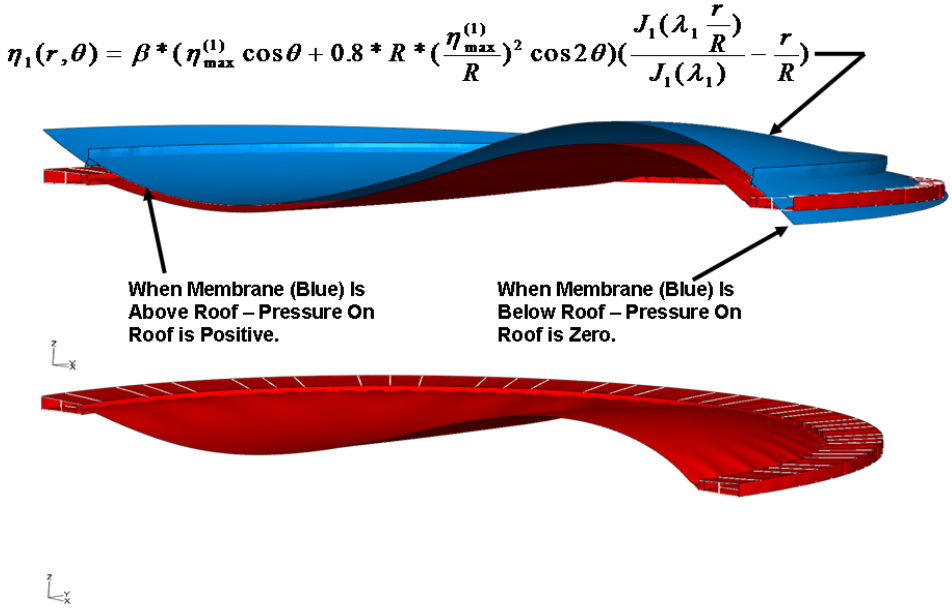

Figure 12. Floating roof w/wo membrane - Mode 1 attenuation factor calculation.

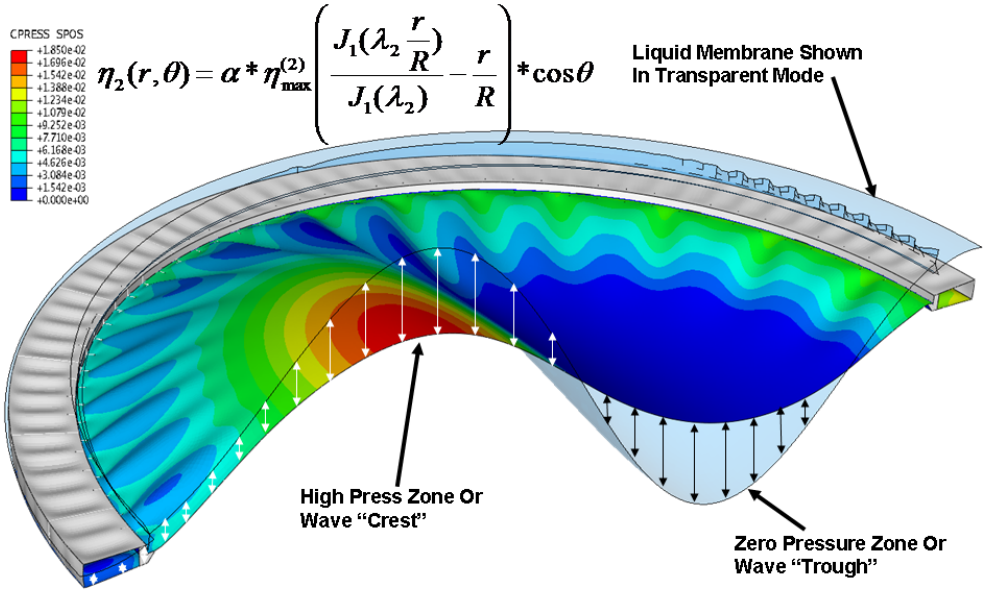

Figure 13. Mode 2 shape & attenuation factor calculation.

4. Calculation of Displacements, Forces, Moments and Stresses

    a. Once the attenuation factors have been calculated for Modes 1 and 2, there are a number of options for determining the displacements, forces, moments and stresses.
    b. The most accurate and technically defensible is to combine the attenuated Mode 1 and Mode 2 displacement shape into a single synthesized deformation pattern.
    c. This is accomplished by calculating the magnitude of displacement for each mode at each point in the pontoon. A square root of the sum of the squares of the magnitude is calculated and then a cosine variation is restored to the pattern.
    d. The synthesized sloshing deformation pattern is then applied to the deck portion of the floating roof first. This displacement pattern reflects the presence of the pontoon on the floating roof. This step calculates the critical radial contraction displacements of the deck on the pontoon.
    e. In the next step, refine the pontoon element mesh for accurate force and stress calculation. Apply the radial contraction from (d), dead weight and buoyancy loads to the pontoon while subjecting the pontoon to the deformations describe in Equation 4.
    f. All calculations are based on large geometric deformations.
    g. Calculate the resulting deflections, forces and stresses in the pontoon under large geometric deformations.
    h. Evaluate critical weld strength in separate detailed analyses.

Analysis of 100 KKL Tank

The concepts above are applied to a 100 KKL located on the Japanese Island of Hokkaido. In 2003, a magnitude 8.0 earthquake (Tokachi-Oki) occurred offshore of Hokkaido in the Kuril Trench which is part of the Pacific Ring of Fire. The earthquake caused extensive damage to numerous storage tanks at a Japanese Refinery on the island. The 100 KKL tank was one of the largest damaged tanks. Critical parameters of the tank and the results of simplified FSL spreadsheet calculations for stress are shown below in Figure 14.

The spreadsheet calculations are based on methods incorporated in the Japanese Fire Service Law (FSL). The law set the minimum requirements to determine if a floating roof required modifications to sustain earthquake loads. The modifications are not defined and the methods could be manipulated to produce the desired result without improving the integrity under earthquake loading.

FSI Model

A finite element model for the tank wall, tank bottom, the contained fluid and the floating roof is used in a dynamic, direct integration fluid-structure interaction (FSI) analysis in ADINA (Kozak, 2008).

1. Assume quake response is symmetrical with respect for the earthquake horizontal direction
2. Assume tank wall and bottom are rigid. These components are primarily affected by the impulsive loads of the contained fluid. Impulsive loads occur in the 2 Hz range whereas the convective 2nd Mode sloshing is in the 0.2 Hz range.

Tank Parameters (100kkl Crude Oil Tank)	
Tank Shell Height	2450 cm
Tank Shell Radius	3910 cm
Maximum Tank Liquid Height	2082 cm
Liquid Density	0.832E-03 kg/cm**3
Pontoon Width	500 cm
Modulus of Elasticity	2.1E+06 2 kgf/cm**2
Material Yield Stress	2500 kgf/cm**2
Freeboard	368 cm
Mode 1 Period @ Max. Liquid Height	10.65 sec
Mode 2 Period @ Max Liquid Height	5.45 sec
Pontoon Area	774.37 cm**2
Moment of Inertia (Theta)	6.93621E+05cm**4
Radius To Pontoon C.G.	3657.4 cm
2 Circumferential Stiffeners	
Pontoon – 42 compartments with Bulk Heads	
3 Stiffening Trusses Per Compartment	

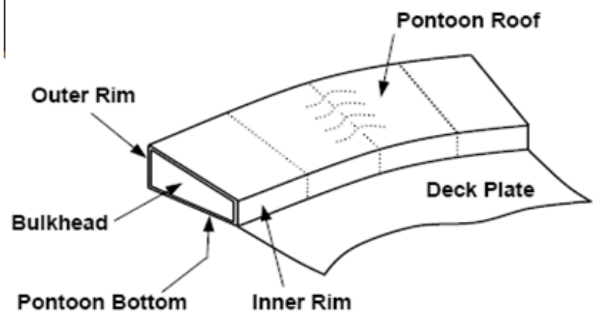

Circumferential Stress (kgf/cm**2)	Outer Rim Lower Corner	Inner Rim Lower Corner
1) Mode 1 Bending	1802	1294
2) Mode 2 Bending	373	423
3) Mode 2 Thrust	2522	2522
4) 2+3	2895	2945
SRSS 1 & 4	3410	3216
% of Yield	136.4%	128.6%

FSL Simplified Hand Calculation Results For Circumferential Stress

Figure 14. Example floating roof tank analysis.

3. Tokachi-Oki earthquake of 2003 is used in the analysis. Only the horizontal (East-West) component of the ground acceleration is used. The acceleration is applied to the tank bottom.
4. Earthquake spectra applied in 3 analyses:
    a. FSI model constrained to respond in the 1st Mode only
    b. FSI model constrained to respond in the 2nd Mode only
    c. Unconstrained FSI model constrained to respond in combination of 1st and 2nd modes
5. FSI model verified with dead weight and frequency analyses.
6. Stiff (compression only) interaction between the floating roof and tank shell wall.

Tank W/o Roof Frequency Analysis

Mode	f (Hz)	Period (sec)	Modal Participation Factors	
			Y	Z
1	0.0939	10.652	64.3%	0.0%
2	0.1340	7.463	0.0%	3.85%
3	0.1534	6.519	0.0%	5.23%
4	0.1615	6.192	0.0%	0.0%
5	0.1832	5.459	0.0%	0.04%
6	0.1834	5.453	2.6%	0.0%

Tank W/ Roof Frequency Analysis

Mode	f (Hz)	Period (sec)	Modal Participation Factors	
			Y	Z
1	0.0937	10.676	64.2%	0.0%
2	0.1384	7.225	0.0%	0.0%
3	0.1535	6.515	0.0%	0.0001%
4	0.1833	5.456	2.5%	0.0%

FSL Equations

Mode 1 = 10.65 **sec**

Mode 2 = 5.45 **sec**

Table 1. FSI vs FSL frequency, mode shape, and participation factor calculation.

Table 1 contains the modal frequency response and participation factors for a floating roof storage tank with and without the roof. The presence of the floating roof has a minor impact on both quantities. The earthquake ground acceleration record used in the time history FSI analysis has been used to generate a pseudo-velocity spectrum (Figure 15). The velocity potential equations require a modal velocity factor for each mode. Figure 15 indicates that for periods of 5.46 and 10.68 seconds the pseudo-velocity values are 237.6 and 70.7 cm/sec respectively.

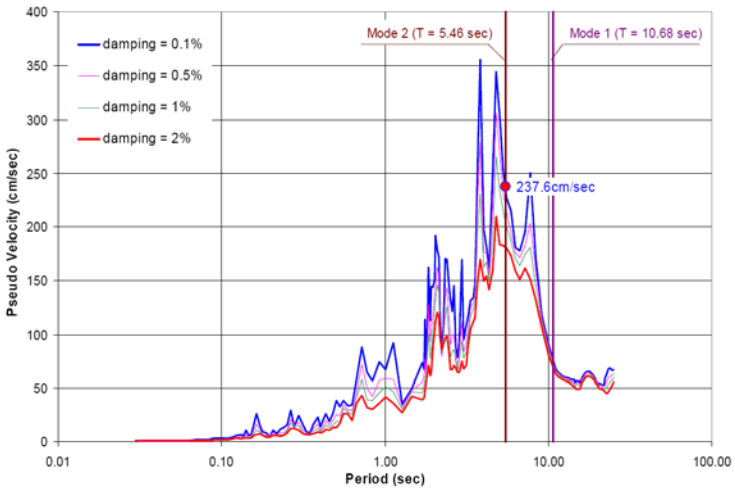

Figure 15. Pseudo velocity spectrum for 2003 Tokachi-Oki earthquake.

The Mode 1 surface oscillation retrieved from the free surface and floating roof analyses are compared in Figure 16. These diagrams match very well which indicates that there is no Mode 1 attenuation due to the floating roof for this tank under Tokachi-Oki ground accelerations.

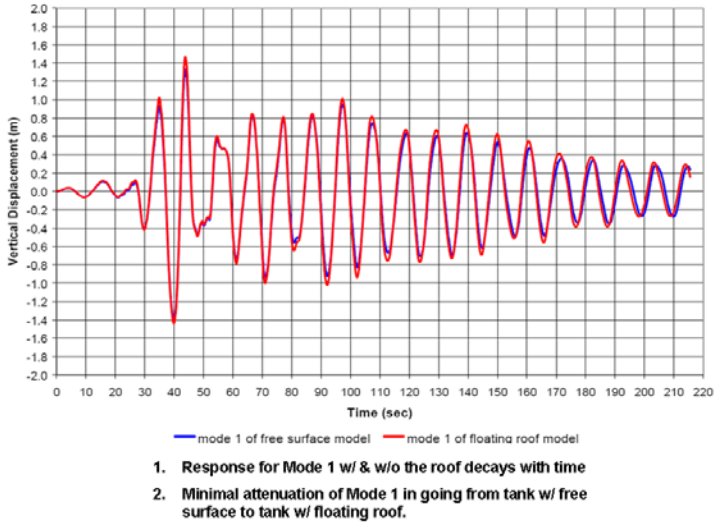

Figure 16. FSI Mode 1 constrained fluid under 2003 Tokachi-Oki ground accelerations.

The FSI results are in good agreement with the CPA. The Contact Pressure Approach predicts a Mode 1 β=1.0, i.e. no attenuation. This agrees with the FSI solution. Comparison of the Mode 2 response in Figure 17 indicates a strong attenuation of the sloshing wave of the free surface due to the floating roof.

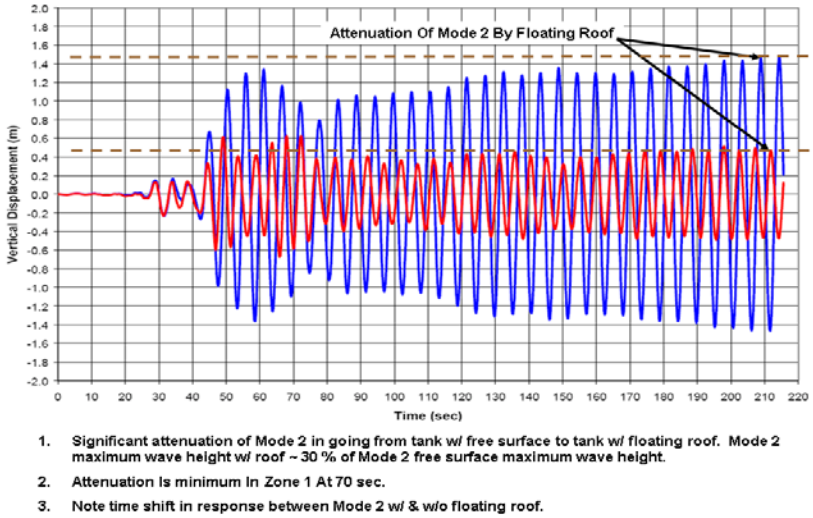

Figure 17. FSI Mode 2 constrained fluid under 2003 Tokachi-Oki ground accelerations.

The Contact Pressure Approach predicts a α=0.2623 based on a velocity spectrum value of 210.8 cm/sec, the maximum allowed in the velocity spectrum specified in the Japanese FSL. The FSI α ranges from 0.275 to 0.32 but corresponds to the pseudo-velocity value of 237.6 cm/sec.

Figure 18 contains the time history response of the total maximum wave height over the entire surface of the floating roof (blue line) and maximum wave heights at the tank wall. Note that total maximum wave height on the roof occurs at different points on the roof in the time domain of the response. The red line mostly overlaps the blue one (total maximum at the wall) which indicates domination of the Mode 1 sloshing. This is confirmed in Figure 19 which demonstrates the total maximum wave height (blue line) and the Mode 1 and Mode 2 contributions (red and green lines respectively

Results

Figure 20 contains a plot of the maximum and minimum force per unit length in the exterior pontoon wall (outer rim) based on the results of the FSI solution. The lower right portion of the figure contains a comparison of the ExxonMobil CPA and the FSI solution at the time the maximum force occurs in the analysis (70.2 sec). The results agree very closely. Due to space restrictions, a limited amount of the results and comparisons are shown. Forces are used in the comparison due to their 1st order accuracy. In addition, the comparison of stresses based on two different Finite Element programs is difficult due to the differences in the element technology and mesh refinement.

Figure 21 contains a summary of the results obtained (in table) for the membrane forces and for the

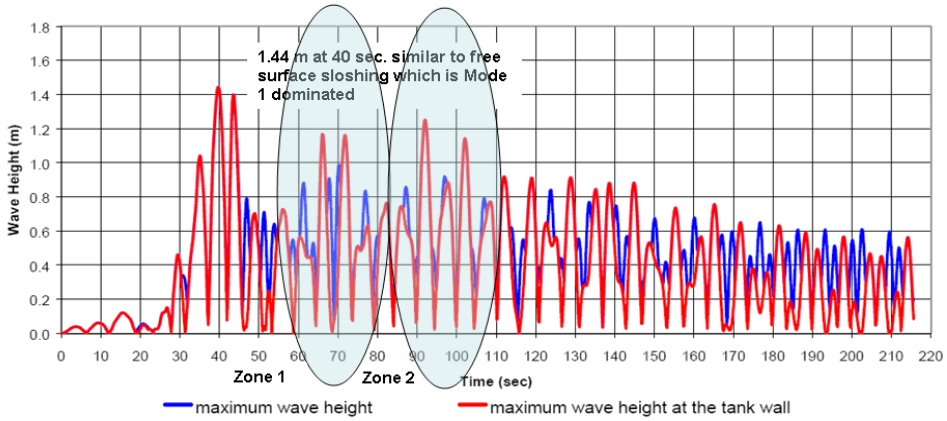

1. **Zone 1 – Early Mode 1 response domination is first affected by growth in Mode 2 response contribution. Mode 1 asserts itself in Zone 2 until its contribution slowly dissipates. Time history analysis w/o the roof identical except zones shift forward slightly in time when roof present.**
2. **Zone 1 generates the most damage in pontoon as Mode 1 and Mode 2 compete for domination of the time history response.**

Figure 18. FSI maximum wave height vs time.

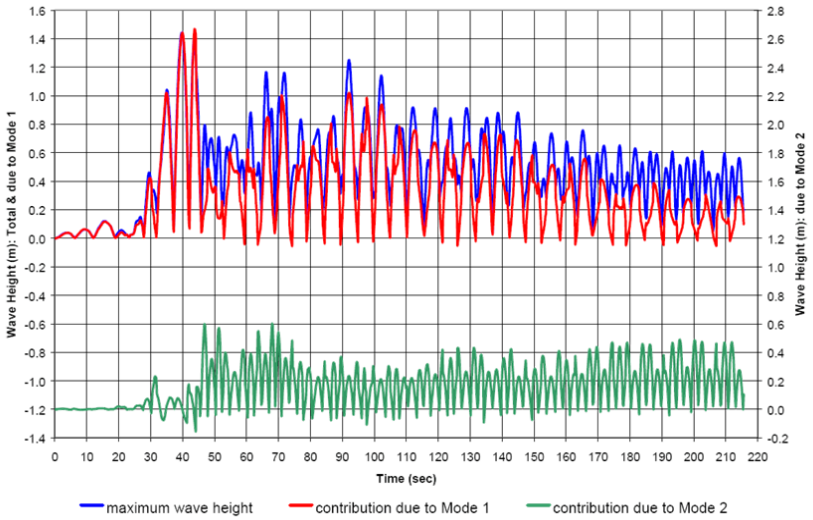

1. **Mode 2 contribution to maximum wave height reaches peak of 60 cm & a minimum of 28 cm over the time history.**

Figure 19. Total maximum wave height - Mode 1 and Mode 2 contributions.

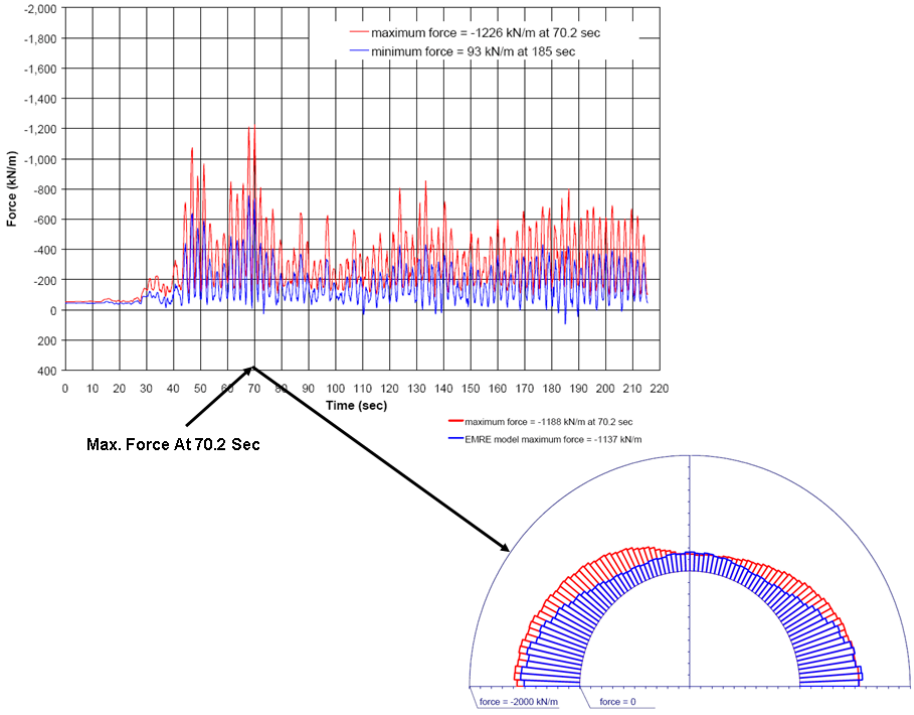

Figure 20. Compressive membrane force in exterior pontoon wall - FSI vs ExxonMobil CPA Method.

total thrust (circumferential) on the pontoon. The results from the two approaches are very close. There are significant differences in the complexity and sophistication of the two approaches. Some of the assumptions retained in the ExxonMobil CPA conform to principles and guidance in the Fire Service Law. The FSI analysis removes most of these assumptions.

The major differences in the two approaches are:

1. ExxonMobil CPA is designed to conform to the basic concepts embedded in the Japanese Fire Service Law. The goal of this work is to gain acceptance from the Japanese Fire Disaster Management Agency to use this approach in lieu of the simple spreadsheet solution. ExxonMobil determined that the spreadsheet approach was not consistently conservative for all tanks and overly conservative for many tanks. An over conservative calculation would result in costly and ineffective modifications to existing roofs.
2. The most significant difference between the ExxonMobil CPA and FSI is that the ExxonMobil CPA is based on the FSL Seismic Design Spectrum which limits the maximum velocity value to 210.8 cm/sec.
3. No modal phase relationships in the ExxonMobil CPA. FSI retains phase relationships.

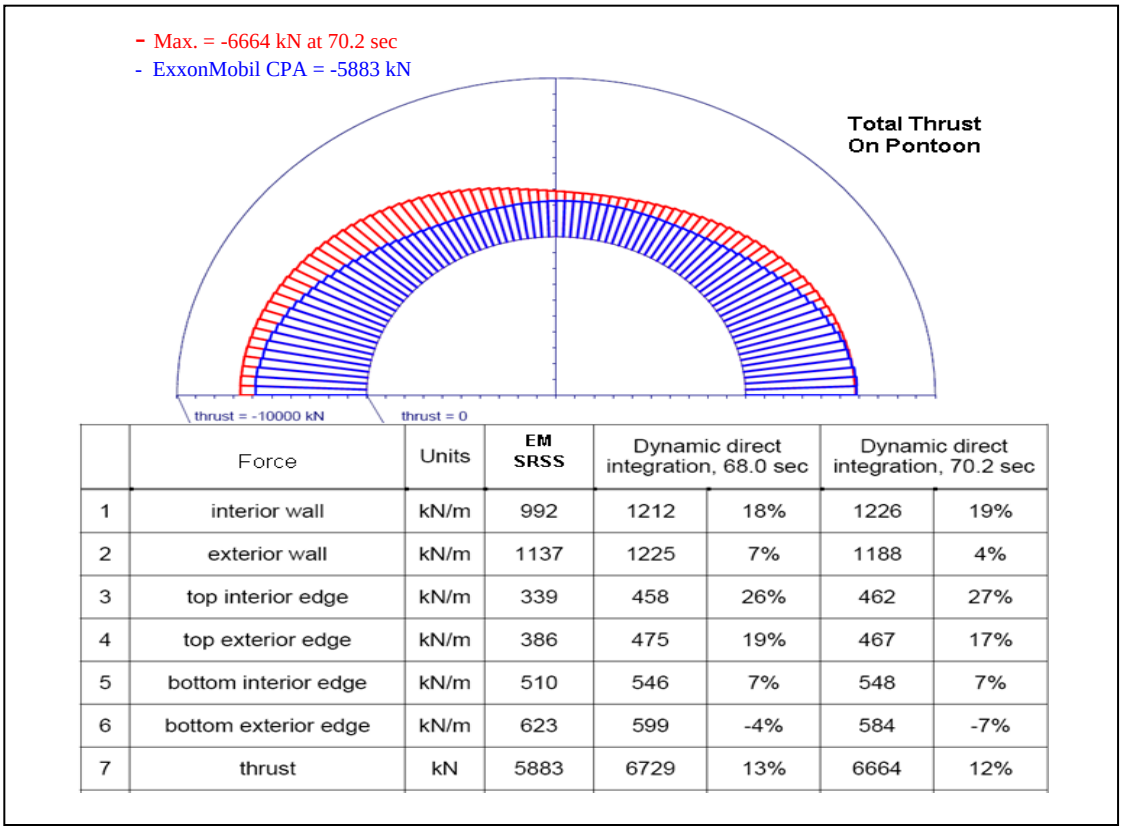

	Force	Units	EM SRSS	Dynamic direct integration, 68.0 sec		Dynamic direct integration, 70.2 sec	
1	interior wall	kN/m	992	1212	18%	1226	19%
2	exterior wall	kN/m	1137	1225	7%	1188	4%
3	top interior edge	kN/m	339	458	26%	462	27%
4	top exterior edge	kN/m	386	475	19%	467	17%
5	bottom interior edge	kN/m	510	546	7%	548	7%
6	bottom exterior edge	kN/m	623	599	-4%	584	-7%
7	thrust	kN	5883	6729	13%	6664	12%

Figure 21. Sloshing force totals in pontoon components - ExxonMobil CPA vs time history analysis.

For the example tank and floating roof, Mode 2 provides the dominant damage mechanism. The differences in the velocity spectrum values inherent in the two approaches can be approximately accounted for by scaling the ExxonMobil CPA results up to the FSI peak velocity spectrum value. Using a scaling factor of 1.14, the results in Figure 18 are adjusted and presented in Table 2.

Table 2. Scaled ExxonMobil CPA results to account for different velocity spectrum values.

Force	Units	EM SRSS	FSI At 68 Sec	FSI At 70.2 sec	Average FSI	Scaled EM	EM/FSI
Interior Wall	kN/m	992	1212	1226	1219	1117	92%
Exterior Wall	kN/m	1137	1225	1188	1207	1280	106%
Top Interior Edge	kN/m	339	458	462	460	382	83%
Top Exterior Edge	kN/m	386	475	467	471	435	92%
Bottom Interior Edge	kN/m	510	546	548	547	574	105%
Bottom Exterior Edge	kN/m	623	599	584	592	702	119%
Thrust	kN	5883	6729	6664	6697	6625	99%

Conclusions

1. ExxonMobil CPA represents a significant reduction in the required modeling and computational effort when compared to a dynamic direct integration fluid structure interaction analysis. It accomplishes this without a significant loss in accuracy.
2. ExxonMobil CPA provides adequate force and stress information to perform detailed evaluation of pontoon components and welds. This information enables structural modifications that improve structural integrity under seismic loading. This is particularly critical to evaluating the adequacy of welds.
3. ExxonMobil CPA uses a seismic design spectrum. FSI requires ground acceleration records and the results are only applicable to the corresponding earthquake. This limits the usefulness to post quake evaluation. CPA can be used for both design and analysis
4. ExxonMobil CPA will enable the development of more comprehensive strain and buckling criteria for evaluating the structural integrity under seismic loading.
5. CPA is currently being extended to the issue of floatation stability due to the flooding of one or more pontoon compartments.

References

1. Cacciatore, Philip J., "Seismic Analysis of Atmospheric Storage Tanks Using The ABAQUS Finite Element Program", ExxonMobil Report EE.256E.2004.
2. Cacciatore, Philip J., L. Magnus Gustafson, Yoichi Ishizaki, Koji Jingu, "Evaluation of the Seismic Response of Floating Roofs on Large Petrochemical Storage Tanks", ExxonMobil Report 2009 MEC 40, May 2009.
3. Guidelines for the Seismic Design of Oil and Gas Pipeline Systems, Committee on Gas and Liquid Fuel Lifelines of the ASCE Technical Council on Lifeline Earthquake Engineering, American Society of Civil Engineers, 1984.

4. Kikuchi, Tsutomu, and Masahiro Mura, "The Sloshing Simulation of Floating Roof Tank", PVP2005-71439, Proceedings of the 2005 ASME Pressure Vessels and Piping Division Conference, July, 2005
5. Kozak, Alexander and Ballard, Thomas A., "ExxonMobil Research and Engineering Company Seismic Analysis of a Liquid Storage Tank Floating Roof, SC Solutions Inc, Task Order No.: 620/4510270251, January, 2008
6. Report of Study to Develop Reasonable Modification Procedures to Satisfy Technical Standard Regarding Relatively Long Period Ground Motion for Facilities Handling Hazardous Materials, Japanese Government Fire Disaster and Management Agency, March 20006. (In Japanese).
7. Yamauchi,Yoshihiko, Kamei, Asamichi, Zama, and Yoshinori Uchida, “Seismic Design of Floating Roof of Oil Storage Tanks Under Liquid Sloshing”, PVP2006-ICPVT11-93280, Proceedings of the 2006 ASME PVP Division Conference, July, 2006.

Acknowledgements

As you might expect, a lot of ExxonMobil people made contributions to this work. In particular, the participation and support provided by the ExxonMobil Asia Area Engineering Office, including the efforts of Tatsuro Ohki-san, Yoicihi Ishizaki-san and Koji Jingu-san have been greatly appreciated. The work done by Ishizaki-san in presenting the complex arguments of this work to the Japanese authorities provided immeasurable value to effort.

ExxonMobil would also like to acknowledge the contributions of Tsutomu Kikuchi, Senior Engineer at Idemitsu Kosan Co. Ltd. for his support and assistance in obtaining relevant tank data and damage photos, Thomas Ballard, formerly of SC Solutions Inc. and his work on the FSI solution, and Benjamin F. Hantz, formerly of ExxonMobil.